terfaces were flat (111) crystal faces. Thus, SLS-grown whiskers shared the crystal habit, growth direction, and interface features of VLS-grown whiskers.

Over the last several years considerable effort has been expended to develop low-temperature solution-phase molecular routes to materials, with the goals of lowering processing temperatures, producing nonthermodynamic crystal structures, and controlling crystal sizes and morphologies (*17*). With some exceptions (*26*), these endeavors have been compromised by the lack of suitable low-temperature crystallization pathways for covalent nonmolecular solids. Analogs to the high-temperature VLS crystallization method have now been found in the domain of low-temperature solution-phase chemistry, possibly opening the way to the low-temperature SLS crystallization of many other covalent solids as fibers, as whiskers, and, when sufficient control is developed, as quantum wires and quantum dots.

REFERENCES AND NOTES

1. A. W. Vere, *Crystal Growth, Principles and Progress* (Plenum, New York, 1987), chap. 1.
2. M. Dugue, J. F. Goullin, P. Merenda, M. Moulin, in *Preparative Methods in Solid State Chemistry*, P. Hagenmuller, Ed. (Academic, New York, 1972), pp. 309–360.
3. M. J. Ludowise, *J. Appl. Phys.* **58**, R31 (1985).
4. R. Didchenko, J. E. Alix, R. H. Toeniskoetter, *J. Inorg. Nucl. Chem.* **14**, 35 (1960); B. C. Harrison and E. H. Tompkins, *Inorg. Chem.* **1**, 951 (1962).
5. A. H. Cowley, P. R. Harris, R. A. Jones, C. M. Nunn, *Organometallics* **10**, 652 (1991).
6. R. S. Wagner and W. C. Ellis, *Appl. Phys. Lett.* **4**, 89 (1964).
7. "Whisker" refers to a filamentary single crystal having a large length:diameter ratio; "fiber" refers to other filamentary structures.
8. E. K. Byrne, L. Parkanyi, K. H. Theopold, *Science* **241**, 332 (1988).
9. T. Douglas, thesis, Cornell University (1991).
10. _____ and K. H. Theopold, *Inorg. Chem.* **30**, 594 (1991).
11. S. C. Goel, M. Y. Chiang, W. E. Buhro, *J. Am. Chem. Soc.* **112**, 5636 (1990).
12. M. A. Olshavsky, A. N. Goldstein, A. P. Alivisatos, *ibid.*, p. 9438; H. Uchida, C. J. Curtis, A. J. Nozik, *J. Phys. Chem.* **95**, 5382 (1991); H. Uchida, C. J. Curtis, P. V. Kamat, K. M. Jones, A. J. Nozik, *ibid.* **96**, 1156 (1992).
13. O. I. Mićić, C. J. Curtis, K. M. Jones, J. R. Sprague, A. J. Nozik, *ibid.* **98**, 4966 (1994).
14. H. Uchida *et al.*, *Chem. Mater.* **5**, 716 (1993).
15. C. B. Murray, D. J. Norris, M. G. Bawendi, *J. Am. Chem. Soc.* **115**, 8706 (1993).
16. M. L. Steigerwald *et al.*, *ibid.* **110**, 3046 (1988), and references therein.
17. W. E. Buhro, *Polyhedron* **13**, 1131 (1994).
18. Phosphine and arsine are highly toxic and must be handled in accordance with proper safety measures. E. Fluck, *Fortschr. Chem. Forsch.* **35**, 1 (1973); W. Braker and A. L. Mossman, *Effects of Exposure to Toxic Gases—First Aid and Medical Treatment* (Matheson Gas Products, East Rutherford, NJ, 1970), pp. 37–38 and 86–96.
19. D. C. Bradley, D. M. Frigo, M. B. Hursthouse, B. Hussain, *Organometallics* **7**, 1112 (1988).
20. R. A. Kovar, H. Derr, D. Brandau, J. O. Callaway, *Inorg. Chem.* **14**, 2809 (1975).
21. R. S. Wagner, in *Whisker Technology*, A. P. Levitt, Ed. (Wiley, New York, 1970), chap. 3; E. I. Givargizov, in *Current Topics in Materials Science*, E. Kaldis, Ed. (North-Holland, Amsterdam, 1978), vol. 1, chap. 3.
22. R. L. Barns and W. C. Ellis, *J. Appl. Phys.* **36**, 2296 (1965); C. M. Wolfe, C. J. Nuese, N. Holonyak Jr., *ibid.*, p. 3790; W. C. Ellis, C. J. Frosch, R. B. Zetterstrom, *J. Cryst. Growth* **2**, 61 (1968); J. J. Nickl and W. Just, *ibid.* **11**, 11 (1971); M. Yazawa, M. Koguchi, K. Hiruma, *Appl. Phys. Lett.* **58**, 1080 (1991); M. Yazawa, M. Koguchi, A. Muto, M. Ozawa, K. Hiruma, *ibid.* **61**, 2051 (1992); M. Yazawa, M. Koguchi, A. Muto, K. Hiruma, *Adv. Mater.* **5**, 577 (1993).
23. E. Kuphal, *J. Cryst. Growth* **67**, 441 (1984).
24. A. R. West, *Solid State Chemistry and Its Applications* (Wiley, New York, 1984), p. 237.
25. _____, *ibid.*, p. 367.
26. E. Ramli, T. B. Rauchfuss, C. L. Stern, *J. Am. Chem. Soc.* **112**, 4043 (1990); S. Dev, E. Ramli, T. B. Rauchfuss, C. L. Stern, *ibid.*, p. 6385; A. F. Hepp, M. T. Andras, S. G. Bailey, S. A. Duraj, *Adv. Mater. Opt. Electron.* **1**, 99 (1992).

27. This research was funded by an NSF Presidential Young Investigator Award (CHE-9158369) to W.E.B., generously supported by Emerson Electric, Eastman Kodak, Monsanto, and Mr. and Mrs. A. H. Homeyer. K.M.H. was supported by a Department of Education Graduate Assistance in Areas of National Need grant.

29 June 1995; accepted 20 October 1995

High Photorefractive Gain in Nematic Liquid Crystals Doped with Electron Donor and Acceptor Molecules

Gary P. Wiederrecht, Beth A. Yoon, Michael R. Wasielewski

Liquid crystalline composite materials have been prepared that are strongly photorefractive. Nematic liquid crystals were doped with both electron donor and electron acceptor molecules that undergo facile, photoinduced, electron transfer reactions to yield mobile ions. A photorefractive gain ratio of 1.88 was observed. This gain ratio was achieved with low applied electric fields (0.4 kilovolts per centimeter) requiring only a 1.5-volt battery and low light intensities (100 milliwatts per square centimeter) in samples 37 to 88 micrometers thick that showed no loss in gain over a 6-month period.

Photorefractive materials hold great promise for optical device applications in the areas of reversible optical holography, noise-free optical image amplification, phase conjugate mirrors, and other optical signal processing techniques (*1*). The photorefractive effect is a change in the refractive index of an electrooptic material that is produced by a space-charge field resulting from photoinduced directional charge transport over macroscopic distances within the material. A pair of coherent laser beams that are crossed in a photorefractive material produce an interference pattern that photogenerates charges in the illuminated regions. These charges migrate by diffusion, often under the influence of an applied electric field, into the dark regions of the interference pattern. The resultant space-charge field modulates the index of refraction of the material, producing a refractive index grating.

Beam coupling between the two crossed laser beams occurs by means of their interaction with the index grating, which is spatially phase-shifted relative to the optical interference pattern. The result is that one beam gains energy at the expense of the other (*2*). This gain is diagnostic for the photorefractive effect in thick or volume gratings and is the basis for many of the applications listed above. A particularly exciting advance in this field came in 1991 with the discovery of photorefractivity in organic polymers (*3*). Subsequently, the performance of organic photorefractive materials improved very rapidly, and at present these materials have higher net photorefractive gain than do their inorganic single crystal counterparts (*2*, *4*, *5*). Such large effects have been achieved through optimization of the charge generation, charge transport, and electrooptic characteristics of the doped polymers. In addition, researchers have decreased the glass transition temperature of the polymers, which permits orientational alignment of the birefringent, nonlinear optical chromophores by a space-charge field within the viscous polymer. This nonlinear electrooptic effect, called the orientational effect, produces an additional large contribution to the total change in the index of refraction (*6*). In fact, the orientational effect makes a greater contribution to the photorefractive gains reported for the most recent polymers than does the traditional linear electrooptic effect (*4*).

On the basis of this information, nematic liquid crystals (LCs) are very attractive substances for use in photorefractive materials because they consist entirely

G. P. Wiederrecht, Chemistry Division, Argonne National Laboratory, Argonne, IL 60439–4831, USA.
B. A. Yoon, Department of Chemistry, Northwestern University, Evanston, IL 60208–3113, USA.
M. R. Wasielewski, Chemistry Division, Argonne National Laboratory, Argonne, IL 60439–4831, and Department of Chemistry, Northwestern University, Evanston, IL 60208–3113, USA.

of long rod-shaped molecules that produce greater bulk birefringence than does a polymer that is merely doped with a birefringent chromophore. Also, LCs have directional order despite their low viscosity, which allows for greater orientational displacement for a given space-charge field. Photorefractive polymeric materials require large electric fields to pole the material to obtain a bulk electrooptic effect, whereas LCs require only a weak electric field to induce directional charge transport and to enhance the quadratic electrooptic effect (6). Finally, many LCs have very little absorption in the visible and near-infrared spectral regions, which minimizes unwanted absorption from the birefringent chromophore. Recently, a photorefractive effect that was derived entirely from orientational ordering within a space-charge field was observed in a nematic LC (7, 8). Space-charge fields within LCs often are a consequence of the Carr-Helfrich effect in these materials (9). The LC 4′-(*n*-pentyl)-4-cyanobiphenyl (5CB) was doped with small amounts of the laser dye rhodamine 6G (R6G), which functioned as the charge generator. These promising results were limited by the low solubility of R6G in 5CB and by inefficient charge generation and charge transport.

Here we report large orientational photorefractive effects in nematic LCs through the systematic addition of both electron donors and electron acceptors that are easily oxidized and reduced, respectively, to yield stable radical ions. Two-beam coupling experiments using two beams of equal intensity for samples as thin as 37 μm resulted in beam amplification or loss of 88%. Photorefractive rise times as short as 40 ms were observed, although they occurred at the expense of photorefractive gain.

The experimental configuration (Fig. 1) used two coherent, 514-nm beams from a continuous-wave Ar^+ laser that were crossed in the sample. The beams were unfocused and had a diameter at the sample of 2.5 mm. Mixtures of 35% (weight %) 4′-(*n*-octyloxy)-4-cyanobiphenyl (8OCB) and 65% 5CB were homeotropically aligned on indium tin oxide (ITO)–coated glass slides by treatment of the ITO with octadecyltrichlorosilane (10). We found superior photorefractive effects in 8OCB-5CB relative to 5CB alone, presumably because of a greater reorientation angle of the 8OCB and 5CB molecules in the lower viscosity LC mixture (11). The birefringence of 8OCB is also slightly greater than that of 5CB (12). The samples were either 37 or 88 μm thick, as determined by a Teflon spacer. Thinner samples permitted stronger electric fields to be applied because hydrodynamic turbulence resulting from charged particle motion between the two ITO plates was reduced (11). A battery and a low-voltage power supply, respectively, were used to apply voltages of up to 1.5 V (88 μm) and 2.5 V (37 μm) to the sample. This resulted in an electric field of up to 0.68 kV/cm for the 37-μm-thick sample versus 0.17 kV/cm for the 88-μm-thick sample. By comparison, electric fields up to 900 kV/cm are used with photorefractive polymer composites (4).

Perylene and and *N*,*N*′-di(*n*-octyl)-1,4,5,8-naphthalenediimide (NI) (13) were chosen as the electron donor and acceptor dopants, respectively, for the following reasons: (i) They are both highly soluble in 8OCB-5CB. (ii) Perylene has a visible absorption that extends to 514 nm (extinction coefficient $\varepsilon = 610\ M^{-1}\ cm^{-1}$), whereas NI has no visible absorption at 514 nm ($\varepsilon < 10\ M^{-1}\ cm^{-1}$). Thus, perylene serves as the charge generator by absorbing 514-nm light and transferring an electron to NI. (iii) Perylene and NI are easily and reversibly oxidized and reduced, respectively, with one-electron oxidation potentials of 0.8 V and −0.5 V, respectively, versus a saturated calomel electrode (14). Given these redox potentials, efficient charge generation in 8OCB-5CB can occur by excitation of perylene to its lowest excited singlet state (S_1), followed by electron transfer from S_1 to NI, resulting in perylene$^+$ and NI^- ions. (iv) The long axes of perylene and NI align along the director of the liquid crystal, which enables the use of relatively high concentrations of perylene and NI without destroying the LC phase of the 8OCB-5CB mixture.

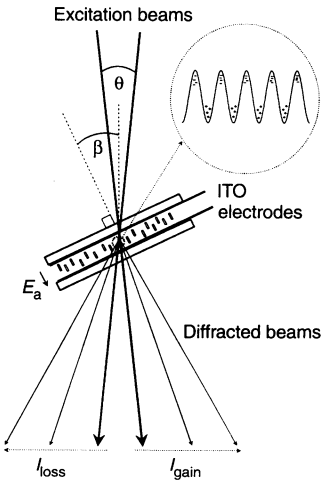

Fig. 1. A schematic of the experimental geometry. The sample is tilted at an angle β = 30° relative to the bisector of the two beams. This permits charge migration along the grating wave vector, which results in a sinusoidal space-charge field. A phase grating results from the influence of the space-charge field on the orientational configuration of the birefringent LC molecules. The wave mixing angle θ varies from 1.9×10^{-3} to 0.15 rad. The beams are p-polarized. E_a is the applied electric field.

The photoconductivity of the perylene and NI mixtures varies between 1.4×10^{-9} to 2.7×10^{-8} $ohm^{-1}\ cm^{-1}$, for an incident light intensity of 1.8 W/cm^2, an applied field of 0.17 kV/cm, and a sample absorption at 514 nm of only 0.5 cm^{-1}. The dark conductivity of these samples was $\cong 10^{-10}$ $ohm^{-1}\ cm^{-1}$. Recently, polymer composites have been prepared that display good photorefractive gains and have optical absorbances of 13 cm^{-1} (4). The LC photoconductivity data normalized to 1 cm^{-1} absorption (Fig. 2A) show that the photoconductivity is up to 50 times greater for the perylene-NI mixture relative to R6G. The quantum yield of mobile charge carriers for the perylene-NI mixture is much better than for the R6G solution, because perylene and NI are easier to oxidize and reduce, respectively, than are R6G and 5CB. No photoconductivity was measurable in samples containing 8OCB-5CB alone or NI alone in 8OCB-5CB. The intensity dependence of the conductivity varies linearly with incident light intensity for these samples (Fig. 2B), indicating that bimolecular ion pair recombination is not important [an $I^{1/2}$ (intensity) dependence] and that the charge transport mechanism in the LC samples may be analogous to that of polymeric systems where photoconductivity is proportional to I (15).

Two-beam coupling experiments were performed with a perylene concentration of

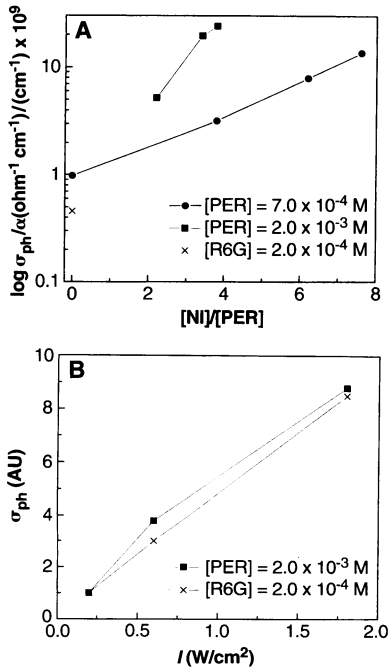

Fig. 2. (**A**) Photoconductivity (σ_{ph}) normalized to an absorption (α) of 1 cm^{-1}, in the perylene- (PER) and NI-doped LC versus a R6G-doped sample. (**B**) The linear increase in the photoconductivity with laser intensity for both samples is shown. AU, arbitrary units.

2.0×10^{-3} M and an NI concentration of 6.8×10^{-3} M in a sample 37 μm thick. The wave mixing angle was $\theta = 6.0 \times 10^{-3}$ rad. Under these conditions, the resulting phase grating is in the Raman-Nath (thin) grating regime, which is known to result in multiple orders of self-diffraction (*16*). The total incident light intensity was only 100 mW/cm^2 (50 mW/cm^2 in each beam). At this intensity, five orders of diffraction were observed. For light intensities of 400 mW/cm^2, as many as eight orders were observed. Observation of two-beam coupling is the definitive criterion for the existence of a photorefractive grating in the thick grating regime (*2*). Beam coupling due to photorefractivity has also been observed in the thin grating regime for semiconductor quantum wells, but the large optical absorption of these materials has precluded net photorefractive gain (*17*). In addition, beam coupling has been observed in thin gratings as a consequence of thermal effects (*18*). In the results presented here, the diffracted beams only appeared in the presence of an applied electric field, eliminating the possibility of beam coupling due to thermal gratings. In addition, the diffracted spots only appeared with extraordinary (p) polarized beams. In the multiple diffraction regime, beam coupling manifested itself as an increase in the intensity of all of the diffracted and undiffracted light from one beam and a corresponding drop in the intensity of the other beam and its diffracted beams.

The photorefractive gain in these LC materials was measured in the following manner. I_1 is the intensity of beam 1 after the sample without beam 2 applied, and I_{12} is the intensity of beam 1 after the sample with beam 2 applied. Correspondingly, I_2 is the intensity of beam 2 after the sample without beam 1 applied, and I_{21} is the intensity of beam 2 with beam 1 applied. In the thin grating regime, the value of I_1 must be corrected because much of the energy in beam 1 is diffracted into higher order beams. After this correction (*19*), the data yield a beam coupling ratio I_{12}/I_1 as high as 1.88. Similar measurements for beam 2, corrected for diffraction, give a beam coupling ratio I_{21}/I_2 as low as 0.11. Thus, the data are in good agreement, indicating that one beam gains 88% of its intensity, whereas the other loses 89% of its intensity. The beam coupling ratio as a function of applied cell voltage is shown in Fig. 3. At these values, the grating fringe spacing (Λ) equals 57 μm and the grating has a rise time of 14 s.

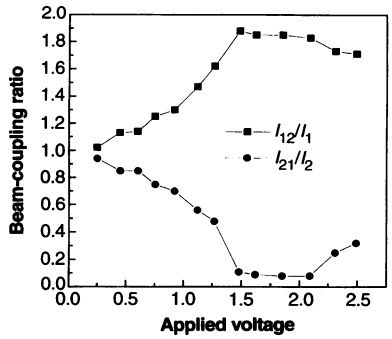

Fig. 3. A plot of beam-coupling ratio versus applied voltage is shown for the beam that gains intensity (■) and the beam that loses intensity (●).

The following relation for quantitatively determining the net photorefractive gain (Γ) from the beam coupling ratio I_{12}/I_1 in the thick grating regime is well known, and assumes that the intensities of the two beams are initially equal (*2*):

$$\Gamma = \frac{1}{D}\left[\ln\frac{I_{12}}{I_1} - \ln\left(2 - \frac{I_{12}}{I_1}\right)\right] - \alpha \quad (1)$$

where I_{12} and I_1 are defined above, α is the absorption coefficient, and D is the overlap length which, in this case, is the optical path length through the sample. However, there is some question as to the validity of this expression in the thin grating regime. Concerning this point, other workers have reported that photorefractive gain in thin samples depends exponentially on sample thickness, even though the diffraction properties of these gratings indicate that they are in the thin grating regime (*8*, *17*). Using $\alpha = 0.5$ cm^{-1}, $D = 37$ μm/cos β = 43 μm, and Eq. 1, we calculate $\Gamma = 640$ cm^{-1}.

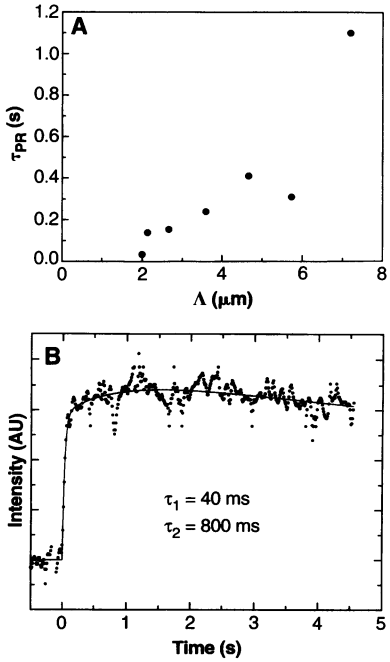

Fig. 4. (**A**) The dependence of grating formation time τ_{PR} on Λ is shown. (**B**) The data illustrate the photorefractive grating rise time τ_1 of 40 ms for Λ = 2 μm. There is a weaker component, τ_2, that makes up 28% of the total amplitude that fits an 800-ms rise time. AU, arbitrary units.

Figure 3 shows that the beam coupling ratio is a nonlinear function of the applied voltage (*8*). The leveling off and subsequent decrease of I_{12}/I_1 and the corresponding changes in I_{21}/I_2 at stronger applied electric fields may be due to hydrodynamic turbulence. The storage time of the sample was on the order of 10 to 30 min, depending on the strength of the grating. Samples containing only 8OCB-5CB or only NI in 8OCB-5CB showed no photorefractivity, whereas samples containing perylene alone in 8OCB-5CB gave beam coupling ratios of 1.25. In the latter case, electron transfer from S_1 of perylene to 8OCB or 5CB or both was weakly endothermic, which precluded efficient charge generation.

We decreased the photorefractive grating formation time by decreasing the fringe spacing, Λ (Fig. 4A) (*20*). At the smallest value for Λ = 2 μm, a rise time of 40 ms was observed (Fig. 4B). This occurs at the expense of photorefractive grating intensity because $\Delta n_e \sim \phi \sim \Lambda$, where Δn_e is the change in the index of refraction along the relevant extraordinary axis, and φ is the reorientational displacement (*8*). The diffraction efficiency at this fringe spacing is 0.025%.

Large photorefractive effects can be achieved within birefringent nematic LCs by doping of the LCs with electron donor and acceptor molecules that undergo facile, excited-state electron transfer reactions to produce mobile ions. The electric field sensitivity, light-intensity dependence, and sample absorbance characteristics of these materials make them attractive candidates for molecular optical devices.

REFERENCES AND NOTES

1. P. Gunter and J. P. Huignard, *Photorefractive Materials and Their Applications*, vols. 1 and 2 (Springer, Berlin, 1988 and 1989); J. Feinberg, *Phys. Today* **41** (no. 10), 46 (1988); _____ and R. W. Hellwarth, *Opt. Lett.* **5**, 519 (1980); J. O. White and A. Yariv, *Appl. Phys. Lett.* **37**, 5 (1980); J. Shamir, H. J. Caulfield, B. M. Hendrickson, *Appl. Opt.* **27**, 2912 (1988); D. Z. Anderson, D. M. Lininger, J. Feinberg, *Opt. Lett.* **12**, 123 (1987); D. D. Nolte, D. H. Olson, G. E. Doran, W. H. Knox, A. M. Glass, *J. Opt. Soc. Am. B* **7**, 2217 (1990).
2. W. E. Moerner and S. M. Silence, *Chem. Rev.* **94**, 127 (1994).
3. S. Ducharme, J. C. Scott, J. Twieg, W. E. Moerner, *Phys. Rev. Lett.* **66**, 1846 (1991).
4. K. Meerholz, B. L. Volodin, Sandalphon, B. Kippelen, N. Peyghambarian, *Nature* **371**, 497 (1994).
5. M. Liphardt *et al.*, *Science* **263**, 367 (1994); Y. Zhang, Y. Cui, P. N. Prasad, *Phys. Rev. B* **46**, 9900 (1992); L. Yu, W. Chan, Z. Bao, S. C. F. Cao, *J. Chem. Soc. Chem. Comun.* (1992), p. 1735.
6. W. E. Moerner, S. M. Silence, F. Hache, G. C. Bjorklund, *J. Opt. Soc. Am. B* **11**, 320 (1994).
7. E. V. Rudenko and A. V. Sukhov, *JETP Lett.* **59**, 142 (1994).
8. I. C. Khoo, H. Li, Y. Liang, *Opt. Lett.* **19**, 1723 (1994).
9. W. Helfrich, *J. Chem. Phys.* **51**, 4092 (1969).
10. I. C. Khoo, *Liquid Crystals: Physical Properties and Nonlinear Optical Phenomena* (Wiley, New York, 1995).
11. P. J. Collings, *Liquid Crystals: Nature's Delicate Phase of Matter* (Princeton Univ. Press, Princeton, NJ, 1990).

12. S. Sen, P. Brahma, S. K. Roy, D. K. Mukherjee, S. B. Roy, *Mol. Cryst. Liq. Cryst.* **100**, 327 (1983).
13. G. P. Wiederrecht, W. A. Svec, M. P. Niemczyk, M. R. Wasielewski, *J. Phys. Chem.* **99**, 8918 (1995).
14. M. R. Wasielewski, R. L. Smith, A. G. Kostka, *J. Am. Chem. Soc.* **102**, 6923 (1980).
15. J. C. Scott, L. Th. Pautmeier, W. E. Moerner, *J. Opt. Soc. Am. B* **9**, 2059 (1992).
16. H. J. Eichler, D. Gunter, D. W. Pohl, *Laser-Induced Dynamic Gratings* (Springer-Verlag, Berlin, 1986).
17. Q. Wang, R. M. Brubaker, D. D. Nolte, M. R. Melloch, *J. Opt. Soc. Am. B* **9**, 1626 (1992).
18. P. Y. Yan and I.-C. Khoo, *IEEE J. Quantum Electron.* **25**, 520 (1989).
19. The value for I_1 in this experiment is given by the relation
$$I_1 = I_0(1 - \eta_T) \quad (2)$$
where I_0 is the intensity in beam 1 after the sample in the absence of diffraction and η_T is the total diffraction efficiency of the grating. For the case of an applied electric field of 0.4 kV/cm, the value for I_1 was 68% (34 mW/cm^2) of the value of I_0 without the electric field. In other words, 32% of the total power lies in the diffracted spots. It is reasonable to consider the 34 mW/cm^2 as the correct value of I_1 for the beam coupling calculations. Subsequently, with both beams incident on the sample, beam 1 was found to increase in intensity to 64 mW/cm^2.
20. A. G. Chen and D. J. Brady, *Opt. Lett.* **17**, 441 (1992).
21. We gratefully acknowledge support from the Office of Computational and Technological Research, Division of Advanced Energy Projects, U.S. Department of Energy, under contract W-31-109-ENG-38.

18 July 1995; accepted 18 October 1995

Efficient Aldolase Catalytic Antibodies That Use the Enamine Mechanism of Natural Enzymes

Jürgen Wagner, Richard A. Lerner,* Carlos F. Barbas III*

Antibodies that catalyze the aldol reaction, a basic carbon-carbon bond-forming reaction, have been generated. The mechanism for antibody catalysis of this reaction mimics that used by natural class I aldolase enzymes. Immunization with a reactive compound covalently trapped a Lys residue in the binding pocket of the antibody by formation of a stable vinylogous amide. The reaction mechanism for the formation of the covalent antibody-hapten complex was recruited to catalyze the aldol reaction. The antibodies use the ε-amino group of Lys to form an enamine with ketone substrates and use this enamine as a nascent carbon nucleophile to attack the second substrate, an aldehyde, to form a new carbon-carbon bond. The antibodies control the diastereofacial selectivity of the reaction in both Cram-Felkin and anti–Cram-Felkin directions.

One of the major goals of organic chemistry is to use the understanding of reaction mechanisms to design new catalysts. This is often not easy because one must address intermediates that are of high energy and complex structure. Antibody catalysts offer an interesting solution to the problem in that they can be programmed by the experimenter to interact with the rate-limiting transition state of a chemical reaction to lower its energy and increase the reaction rate (*1*), but even here catalyst design is usually limited to the more global aspects of the transition state rather than the detailed reaction mechanism. Thus, while one can deal with high-energy charges, stereoelectronic, and geometrical features that appear along the reaction coordinate, the organization of multiple complex reaction intermediates remains difficult.

For some reactions, the problem of complex intermediates may be solved by using relatively reactive compounds rather than the more usual inert antigens to immunize animals or select antibodies from libraries such that the process of antibody induction involves an actual chemical reaction in the binding site (*2*). This same reaction then becomes part of the catalytic mechanism when the antibody interacts with a substrate that shares chemical reactivity with the antigen used to induce it. To test these ideas, we have studied the aldol condensation which is, arguably, the most basic C–C bond forming reaction in chemistry and biology. A variety of effective reagents have been developed to control the stereochemistry of the aldol, but these reagents are stoichiometric and require preformed enolates and extensive protecting-group chemistry (*3*). Recently, catalytic aldol reactions that use preformed enolates have been developed, including the Mukaiyama cross-coupling aldol (*4*). A number of enzymes catalyze the aldol condensation, and although much is understood about their mechanism (*5*) they accept a limited range of substrates (*6*). Thus, our goal was to induce antibodies that use the reaction mechanisms that give aldolases their efficiency but that take advantage of the range of substrates and stereochemical specificities available with antibodies.

Two mechanistic classes of aldolase enzymes have evolved (*7*). Class I aldolases utilize the ε-amino group of a Lys in the active site to form a Schiff base with one of the substrates, which activates the substrate as an aldol donor. Class II aldolases are metalloenzymes that facilitate enolate formation by coordination to the substrate's carbonyl oxygen. We chose class I aldolases as our model (Fig. 1A). The reaction is bimolecular and proceeds through covalent catalysis through multiple intermediates. An iminium ion or Schiff base forms that acts as an electron sink, which lowers the activation energy (E_a) for proton abstraction from the Cα atom and subsequent enamine formation. The enamine acts as the carbon nucleophile, or aldol donor, which reacts with an aldehyde electrophile, the aldol acceptor, to form a new C–C bond. The Schiff base is then hydrolyzed and the product is released (in this case, a β-hydroxy ketone). The essence of the mechanism is the formation of the enamine, which is the nascent carbon nucleophile. Although transition state models have been proposed for aldol reactions involving metals (*8*), models for the enamine case remain to be studied.

We designed haptens that could both trap the requisite Lys residue in the active site to then form the essential enamine intermediate and induce the appropriate binding sites for the two substrates to overcome the entropic barrier intrinsic to this bimolecular reaction. The simple 1,3-diketone hapten **1** provides elements of both a chemical and entropic trap (Fig. 1B). In water, the keto-form of the hapten shown predominates over the enol-form at a 3:1 ratio (*9*). The reaction coordinates of the aldol addition and the reaction mechanism expected when the hapten interacts with some antibodies share several common intermediates. In both cases, a tetrahedral carbinolamine intermediate forms that dehydrates to afford the cationic iminium that tautomerizes to the enamine. It was expected that antibodies induced according to the haptenic reaction mechanism would stabilize the analogous transition states and cationic intermediates along the reaction coordinate of the aldol reaction. The driving force for the reaction of the 1,3-diketone hapten with the antibody is the formation of a stable covalent vinylogous amide or conjugated enamine between the hapten and the ε-amino group of Lys. Calculations that make use of the Woodward rules for enones indicated that the vinylogous amide would have an absorption maximum in the ultraviolet (UV) that would allow for its identification, λ_{max} = 318 nm (*10*). The stability and spectral characteristics of this type of compound were previously noted in the studies of acetoacetate decarboxylase by Westheimer and co-workers (*11*). We expected an entropic advantage by incorporation of the second substrate (aldol acceptor) in the diketone chemical trap. Entropic effects could provide as much as 10^8 to 10^{11} to

Departments of Chemistry and Molecular Biology, Scripps Research Institute, 10666 North Torrey Pines Road, La Jolla, CA 92037, USA.

*To whom correspondence should be addressed.